Biophysics and Physicobiology

Special Issue: Recent Advances in Retinal Protein Research

Regular Article (Invited)

Protein dynamics of a light-driven Na$^+$ pump rhodopsin probed using a tryptophan residue near the retinal chromophore

Akihiro Otomo[1,2,3], Misao Mizuno[1], Keiichi Inoue[4], Hideki Kandori[5], Yasuhisa Mizutani[1]

[1] *Department of Chemistry, Graduate School of Science, Osaka University, Toyonaka, Osaka 560-0043, Japan*

[2] *Present address: Department of Life and Coordination-Complex Molecular Science, Institute for Molecular Science, National Institutes of Natural Science, Okazaki, Aichi 444-8787, Japan*

[3] *Present address: Department of Functional Molecular Science, School of Physical Science, SOKENDAI, Hayama, Kanagawa 240-0193, Japan*

[4] *The Institute for Solid State Physics, The University of Tokyo, Kashiwa, Chiba 277-8581, Japan*

[5] *Department of Life Chemistry, Graduate School of Science, Nagoya Institute of Technology, Nagoya, Aichi 466-8555, Japan*

Direct observation of protein structural changes during ion transport in ion pumps provides valuable insights into the mechanism of ion transport. In this study, we examined structural changes in the light-driven sodium ion (Na$^+$) pump rhodopsin KR2 on the sub-millisecond time scale, corresponding with the uptake and release of Na$^+$. We compared the ion-pumping activities and transient absorption spectra of WT and the W215F mutant, in which the Trp215 residue located near the retinal chromophore on the cytoplasmic side was replaced with a Phe residue. Our findings indicated that atomic contacts between the bulky side chain of Trp215 and the C20 methyl group of the retinal chromophore promote relaxation of the retinal chromophore from the 13-*cis* to the all-*trans* form. Since Trp215 is conserved in other ion-pumping rhodopsins, the present results suggest that this residue commonly acts as a mechanical transducer. In addition, we measured time-resolved ultraviolet resonance Raman (UVRR) spectra to show that the environment around Trp215 becomes less hydrophobic at 1 ms after photoirradiation and recovers to the unphotolyzed state with a time constant of around 10 ms. These time scales correspond to Na$^+$ uptake and release, suggesting evolution of a transient ion channel at the cytoplasmic side for Na$^+$ uptake, consistent with the alternating-access model of ion pumps. The time-resolved UVRR technique has potential for application to other ion-pumping rhodopsins and could provide further insights into the mechanism of ion transport.

Key words: time-resolved resonance Raman spectroscopy, microbial rhodopsin, sodium ion pump, alternating-access model

---

◄ *Significance* ►

Elucidation of protein conformational changes associated with ion transport in ion pumps is important for understanding the mechanism of their functions. We demonstrate the protein dynamics occurring during Na$^+$ transport in the light-driven Na$^+$ pump KR2 using time-resolved ultraviolet resonance Raman spectroscopy. The environment around Trp215 in the vicinity of the retinal chromophore becomes less hydrophobic during ion uptake and then returns to its original hydrophobic environment to prevent the backflow of Na$^+$. These findings are consistent with the alternating-access model of ion pumps, indicating that our method is a powerful tool for elucidating ion transport mechanisms in ion pumps.

Corresponding author: Yasuhisa Mizutani, Department of Chemistry, Graduate School of Science, Osaka University, 1-1, Machikaneyama, Toyonaka, Osaka 560-0043, Japan. ORCID iD: https://orcid.org/0000-0002-3754-5720, e-mail: mztn@chem.sci.osaka-u.ac.jp

Introduction

Membrane transporters are essential proteins for cell survival and cellular homeostasis. In particular, active ion pumps, which transport ions against their concentration gradient, are crucial to generating the ion motive force necessary for ATP synthesis, flagellar motility, secondary transport, and more. The alternating-access model is widely accepted as the means by which ion pumps achieve unidirectional active ion transport. In this model, sequential protein conformational changes are activated by stimuli that alternately open and close gates for transport substrates [1]. Microbial rhodopsins are a family of light-driven active ion pumps which possess a retinal molecule as a chromophore inside a protein moiety composed of seven transmembrane helices (Figure 1) [2,3]. The retinal chromophore is covalently bound to a lysine residue to form a Schiff base, which undergoes photoisomerization by absorbing light. Since the

Figure 1 Protein structure of KR2 [PDB ID: 4xto]. An enlarged view shows the retinal chromophore and Trp215.

retinal chromophore is well packed in a hydrophobic binding pocket, photoisomerization induces a series of global protein conformational changes called the photocycle, which enables active ion transport [4,5].

Recent metagenomic analyses have uncovered various types of ion-pumping rhodopsins, including an outward Na^+ pump (NaR) [6], an inward H^+ pump [7,8], and an inward SO_4^{2-} pump [9], in addition to the classical outward H^+ pump [10] and inward Cl^- pump [11]. A report in 2013 described the first NaR, *Krokinobacter* rhodopsin 2 (KR2), [6,12]. KR2 is a remarkable ion-pumping rhodopsin and can transport Na^+, Li^+, and in the absence of these ions, H^+ [6]. Interestingly, several mutations to KR2 allow the protein to pump K^+ and Cs^+ outward and Cl^- inward [13-16], indicating that the protein structure of KR2 has the potential to transport a variety of ion species. This feature is related to the evolutionary origin of the NaRs, as discussed previously [15,17]. Furthermore, KR2 is expected to be an optogenetic silencer [13,18]. Less photo-invasive modifications have been developed by replacing amino acid residues around the retinal chromophore [19]. Therefore, investigation of the unidirectional Na^+ pump mechanism of KR2 is essential for understanding ion selectivity in ion-pumping rhodopsins and for their development as tools in optogenetics applications.

KR2 forms a pentameric structure in lipid membranes and in detergent micelles in the presence of Na^+ [20,21]. The photocycle of KR2 that allows Na^+ transport from the cytoplasmic to the extracellular side proceeds as follows [6,12]. In the unphotolyzed state, the retinal Schiff base is protonated and is in the all-*trans* configuration. When KR2 absorbs visible light of around 525 nm, the retinal chromophore isomerizes from all-*trans* to 13-*cis* and forms the K intermediate through the earliest J intermediate. In the M intermediate, which is in equilibrium with the L intermediate, the retinal Schiff base is deprotonated, and the H^+ is relocated to the counterion, aspartate 116 (Asp116) [13,22]. Since Na^+ should pass near the retinal Schiff base, H^+ transfer to Asp116 is essential to avoid charge repulsion. Several studies have demonstrated that the uptake of Na^+ from the cytoplasm into the protein occurs in the M-to-O transition [23,24]. Na^+ is then released from the cell as the retinal chromophore relaxes to the unphotolyzed state. Thus, in KR2, the ions taken up are released within the same cycle, in contrast to canonical ion-pumping rhodopsins [12]. The protein dynamics of the O intermediate in which Na^+ uptake and release occur will therefore provide insights into the Na^+ transport mechanism specific to KR2. Two crystal structures of the O intermediate have recently been reported by separate research groups which identified the transient Na^+-binding site inside the protein [25,26]. However, the positions of the binding sites are different in the two structures, and the configurations of the retinal chromophore are different. These inconsistencies may be due to differences in the oligomeric state of the protein used for crystal preparation [25,26]. Thus, further studies directly observing the structural changes in the O intermediate are required.

Here, we used time-resolved ultraviolet resonance Raman (UVRR) spectroscopy to observe structural changes in the O intermediate of KR2 solubilized with a detergent. This technique provides resonantly selective Raman spectra of tryptophan (Trp) and tyrosine (Tyr) residues in proteins [27,28]. We examined wild-type (WT) KR2 and the W215F mutant, in which Trp215, widely conserved in microbial rhodopsins [2], is replaced by phenylalanine (Phe). Trp215 is located on the cytoplasmic side near the retinal chromophore (Figure 1) and is believed to be a mechanical transducer during function, as demonstrated for other ion-pumping rhodopsins [2,29-31]. Ion pump activity and transient absorption spectroscopy indicated that the atomic contact between the bulky side chain of Trp215 and the C20 methyl group of the retinal facilitates relaxation from the O intermediate to the unphotolyzed state. Our time-resolved UVRR spectra showed
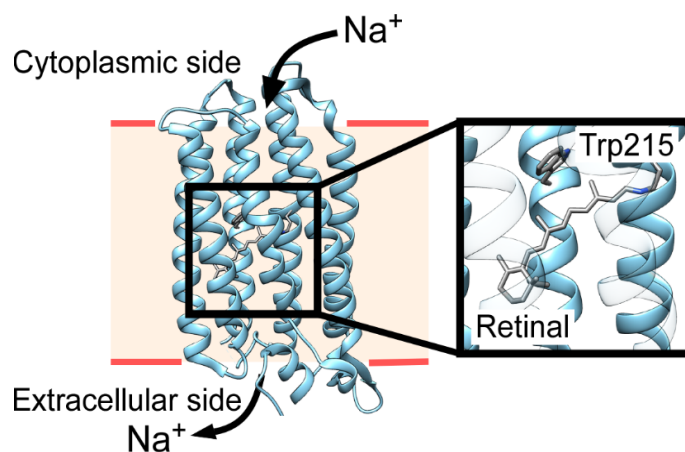
that the environment around Trp215 becomes less hydrophobic at 1 ms, when the population of the O intermediate is at its maximum, and returns to its original hydrophobic state in the transition from the O intermediate to the unphotolyzed state. These conformational changes are associated with Na^+ uptake from the cytoplasm and prevention of Na^+ backflow, consistent with the alternating-access model.

Materials and Methods

Sample Preparation

The expression plasmid for WT KR2 was constructed as described previously [21]. The plasmid for W215F expression was constructed using PCR-based site-directed mutagenesis with a PrimeSTAR Mutagenesis Basal Kit (Takara Bio Incorporated) by following the standard protocol. The KR2 samples were prepared as described previously [21,22]. Briefly, both WT and the W215F mutant of KR2 with a six-histidine tag at the C-terminus were expressed in *Escherichia coli* (*E.coli*) strain C41 (DE3) cells from the expression plasmid pET21a. Cells were cultivated in 2×YT medium containing 50 mg/L ampicillin, then 1.0 mM isopropyl-β-thiogalactopyranoside was added as an inducer at mid-logarithmic phase together with 10 μM all-*trans*-retinal (Toronto Research Chemicals) for 3 h at 37°C. Cells were suspended in suspension buffer (50 mM Tris-HCl (pH 8.0) with 5 mM $MgCl_2$) and then disrupted by ultrasonication. The membrane fraction was collected by ultracentrifugation (109,000×*g*, 60 min at 4°C). After homogenizing the precipitate, the protein was solubilized with 1.5% *n*-dodecyl-β-$_D$-maltoside (DDM) (Dojindo, D316) in solubilization buffer (20 mM MES (pH 6.5) with 300 mM NaCl and 5 mM imidazole) at 4°C overnight. The insoluble fraction was removed by ultracentrifugation (109,000×*g*, 60 min at 4°C), and the supernatant was loaded on a cobalt ion affinity column (GE Healthcare, HiTrap Talon) equilibrated with buffer W1 (20 mM MES (pH 6.5) with 300 mM NaCl, 50 mM imidazole, and 0.1% DDM). After washing with 5 column volumes of buffer W1, KR2 was eluted with buffer E1 (20 mM MES (pH 7.5) with 500 mM imidazole and 0.1% DDM). The colored fractions were collected and loaded on an anion exchange column (GE Healthcare, HiTrap Q HP) and eluted using a gradient of buffer W2 (50 mM Tris-HCl (pH 8.0) with 0.1% DDM) and buffer E2 (50 mM Tris-HCl (pH 8.0) with 1 M NaCl and 0.1% DDM). The buffer in the protein samples was replaced with observation buffer (50 mM Tris-HCl (pH 8.0) with 10 mM NaCl, 300 mM Na_2SO_4, and 0.1% DDM) using a centrifugal filter (Merck Millipore, Amicon Ultra 30 K unit) for spectroscopic measurements. The sample concentration was adjusted to 20 μM.

Ion Transport Measurements

E. coli cells expressing WT and W215F were collected by centrifugation (4,800×*g*, 2 min at 20°C), washed three times (10 mM NaCl, 300 mM Na_2SO_4, and 5% sucrose) and then suspended in the same solution for ion transport activity measurements. The cell suspension was illuminated using a Xe lamp (Asahi Spectra Co., Ltd. MAX-03) through a band-pass filter (OptoSigma, Y48) and a cold filter (OptoSigma, CLDF-50S) at 20°C for 2.5 min. Light-induced pH changes were monitored with a pH meter (Horiba, F-72). The same measurement was performed after adding 10 μM carbonyl cyanide 3-chlorophenylhydrazone (CCCP), a protonophore.

Laser-Flash Photolysis Measurements

Transient absorption spectra were obtained by a laser-flash photolysis system comprising a Xe arc lamp (Hamamatsu Photonics, L8004-01) as a white probe light source, a frequency-doubled Q-switched Nd:YAG laser (Continuum, Minilite) as the 532 nm pump pulse (7 ns, 300 μJ), and a multichannel analyzer equipped with an image intensifier (Hamamatsu Photonics, PMA-12). The repetition frequency of the pump pulse was adjusted in the range between 0.5 and 10 Hz in response to the lifetime of the photocycle of each sample. A digital delay generator (Stanford Research Systems, DG-535) was used to control the timing between the pump pulse and the gate opening of the detector. The sample solution was circulated by a peristaltic pump (ATTO, Bio-Minipump AC-2120). A rectangular-shaped quartz cell with a cross-sectional area of 4 mm^2 (1 mm × 4 mm) was used as the sample cell. The transient absorption changes were calculated by the intensity ratio between the transmitted probe light with or without pump pulse irradiation.

Visible Resonance Raman Measurements

Resonance Raman (RR) measurements of the retinal chromophore of KR2 were performed as described previously [21,22]. Briefly, a single-frequency CW DPSS laser (Cobolt, 04-01 Samba) was used as the probe light at 532 nm. Purified WT and W215F suspended in the observation buffer were placed in a 10 mmϕ glass NMR tube, used as a rotating cell. The Raman scattered light from the sample was collected into a single spectrograph (HORIBA Jobin Yvon, iHR320) and detected with a liquid nitrogen-cooled CCD camera (Roper Scientific, PyLon: 400BeX-VISAR). Raman shifts were calibrated using the Raman bands of acetone, cyclohexane, and toluene, and the calibration error was within 1 cm^{-1}. Measurements were performed at room temperature. To avoid spectral contamination of the long-lived photointermediates, the probe power and rotation speed were set to 125 μW and 750 rpm, respectively.

Time-Resolved UVRR Measurements

Time-resolved UVRR spectra were measured using the dual-beam rapid-flow method using 233 nm probe and 532 nm pump lights, as described previously [30]. The 233-nm probe light was the fourth harmonic of the output of an Nd:YLF-pumped Ti:sapphire laser (Photonics Industries, TU-L). The 135° Raman backscattered light from the sample was detected with a liquid nitrogen-cooled CCD camera (Roper Scientific, Spec-10: 400B/LN-SN-U) equipped with a single spectrograph (HORIBA Jobin Yvon, iHR550) with a 2400-grooves/mm, 400-nm blazed grating. A custom-made prism spectrometer (Bunkoukeiki) was placed before the spectrograph to remove Rayleigh scattered light. Raman shifts were calibrated by the Raman bands of 2-propanol, ethanol, and acetone, and the calibration error was within 1 cm^{-1}. The sample solution was circulated in a rectangular-shaped quartz cell with a cross section of 4 mm^2 (1 mm × 4 mm) using a liquid transfer pump (Cole-Parmer Instrument Company, Masterflex Peristaltic Pump 6-600 RPM). The circulated sample solution was chilled on ice in order to moderate damage by motor heat or UV irradiation. Each measurement was conducted using 40 mL of purified protein solution. The flow rate was controlled by a speed controller set to 150 mL/min. Pumping was achieved using 532-nm cw light (Cobolt, 04-01 Samba) and the 233-nm and 532-nm beams were independently focused onto the flow cell. The timing between the UV probe and the visible pump lights was controlled by changing the spatial irradiating position of the pump beam using a computer-controlled actuator. The temperature at the light irradiation point in the cell was approximately 10 °C. The width of the 532-nm pump beam was 115 μm (FWHM) and the width of the 233 nm probe beam was set to be narrower than that of the pump beam. The time resolution of the measurements was higher than 180 μs.

Results

Biochemical and Spectroscopic Properties of WT and the W215F Mutant

Figure 2A shows the ion transport activity of *E. coli* cells expressing WT and the W215F mutant of KR2 as monitored by light-induced pH changes. Both WT and W215F showed pH increases during light irradiation. The initial slope for W215F was smaller than that for WT, indicating that the W215F mutation decreased pumping activity. The pH changes were canceled by turning off the light and enhanced by adding the protonophore CCCP. This behavior is typical of the light-driven Na$^+$ pumping rhodopsins because outward Na$^+$ transport induces uptake of H$^+$ to balance the membrane potential, and secondary H$^+$ uptake is accelerated by the protonophore [6]. Thus, the present results indicate that the W215F mutant pumps Na$^+$ as well as WT does, albeit with less activity. We then investigated the spectroscopic features of purified WT and W215F solubilized with the detergent DDM. Figure 2B represents the absorption spectra of WT and W215F. The maximum absorption wavelength of WT and W215F was 526 and 524 nm, respectively. The visible RR spectra of the retinal chromophore of the unphotolyzed state upon irradiation with a 532-nm probe light are shown in Figure 2C. The RR bands at 1640–1642, 1532–1577, 1165–1244, and 824–971 cm^{-1} are assigned to the C=N stretching [v(C=N)] mode, C=C stretching [v(C=C)] modes, C-C stretching [v(C-C)] modes, and hydrogen out-of-plane (HOOP) bending modes, respectively [21,22,32-35]. It is well established that the intensity and frequency of these RR bands are good markers of the retinal chromophore and its binding-pocket structures [34,35]. As shown in Figures 2B and C, the absorption maximum wavelengths and frequencies of the RR bands of the retinal chromophore were almost the same for WT and W215F. These results indicate that the structures of the retinal chromophore and the binding pocket in the unphotolyzed state are essentially unaffected by the W215F mutation.

Transient absorption spectra were collected to investigate the kinetics of each photointermediate in the photocycle. Figure 3A shows the difference absorbance spectra of WT and W215F at each delay time ranging from 350 to 700 nm. The photocycle of WT was almost complete at 50 ms, as reported previously [6,22], whereas W215F required more than 900 ms to recover to the unphotolyzed state. The relatively long photocycle of W215F is consistent with the low Na$^+$ pump activity shown in Figure 2A. The positive band observed around 600 nm in the later part of the photocycle corresponds to the O intermediate. Figure 3B represents the time courses of the difference absorbance of the O intermediate for WT and W215F. The plots were fitted well by three exponential equations assuming the decay of the earlier K/L intermediate and the formation and decay of the O intermediate. The obtained time constants of the O intermediate of WT and W215F are shown in Table 1. The time constant of the formation of the O intermediate was comparable for WT and W215F. By contrast, the time constant of the decay in W215F was significantly larger than that in WT, indicating that the W215F mutation resulted in prolonged relaxation of the retinal chromophore.

Time-Resolved UVRR Spectra of WT and the W215F Mutant

Figure 4A shows a UVRR spectrum of WT obtained by only irradiating with the 233-nm probe light (black trace), and of the pump-induced difference spectra (red traces). Excitation at 233 nm enhances the Raman intensities of Trp and Tyr residues in proteins [36,37]. The difference spectra were calculated using the SO$_4^{2-}$ band at 980 cm^{-1} as the internal intensity standard to correct for self-absorption effects. The UVRR bands in the probe-only spectrum arise from Trp (W1,
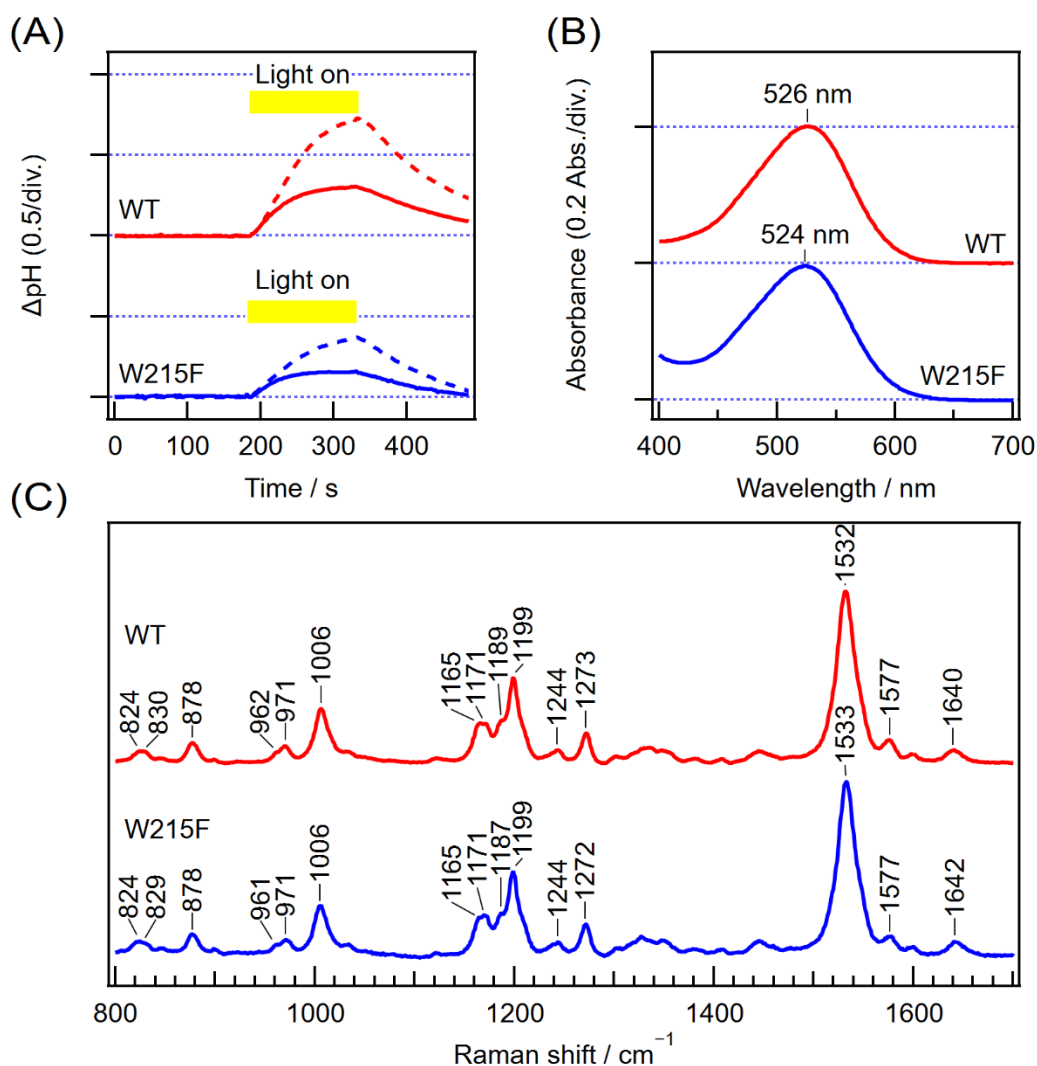
Figure 2 (A) Ion pump activity of *E. coli* cells expressing WT (red) and the W215F mutant (blue) of KR2 suspended in 10 mM NaCl, 300 mM Na_2SO_4, and 5% sucrose. Light exposure time is shown by the yellow bars. Light-induced pH changes were monitored without (solid lines) and with (dotted lines) CCCP. (B) Absorption spectra of purified WT (red) and W215F (blue). (C) Visible resonance Raman spectra of WT (red) and W215F (blue) probed by 532 nm laser light. The spectrum of the buffer and the emission background were subtracted.

benzene ring stretching; W3, C_γ–$C_{\delta 1}$ stretching; W7, $N_{\epsilon 1}$–$C_{\epsilon 2}$ stretching showing a doublet; W16, out-of-phase ring breathing; and W18, in-phase ring breathing) and Tyr (Y8a, ring stretching; and Y9a, C–H in-plane bending) residues [27]. The pump-induced difference spectra from −0.5 ms to 8 ms cover the formation and decay of the O intermediate (Table 1). In the difference spectra, intensity changes for the W7 (1343 and 1359 cm^{-1}), W16 (1011 cm^{-1}), and W18 (764 cm^{-1}) bands and the frequency shift for the W3 (1554 cm^{-1}) and Y9a (1176 cm^{-1}) bands were observed. These spectral changes reflect structural change in the protein around the Trp and Tyr residues during the photocycle [30,31,38,39].

Table 1 Time constants of the formation and decay of the O intermediate

	Formation/ms	Decay/ms
Wild type	0.39 ± 0.03	6.3 ± 0.2
W215F	0.40 ± 0.06	99.1 ± 12.2

Figure 5A shows temporal relative intensity changes of the W16 and W18 bands of WT. Both bands initially decreased in intensity, with a maximum relative change at 1 ms, and then recovered. Intensity recovery in the range from 1 to 8 ms was best fit by a single exponential function (Figure 5A, line). The obtained time constants for the W16 and W18 bands were 10.6 and 9.2 ms, respectively. The W16 and W18 bands reflect the hydrophobic environment around Trp residues
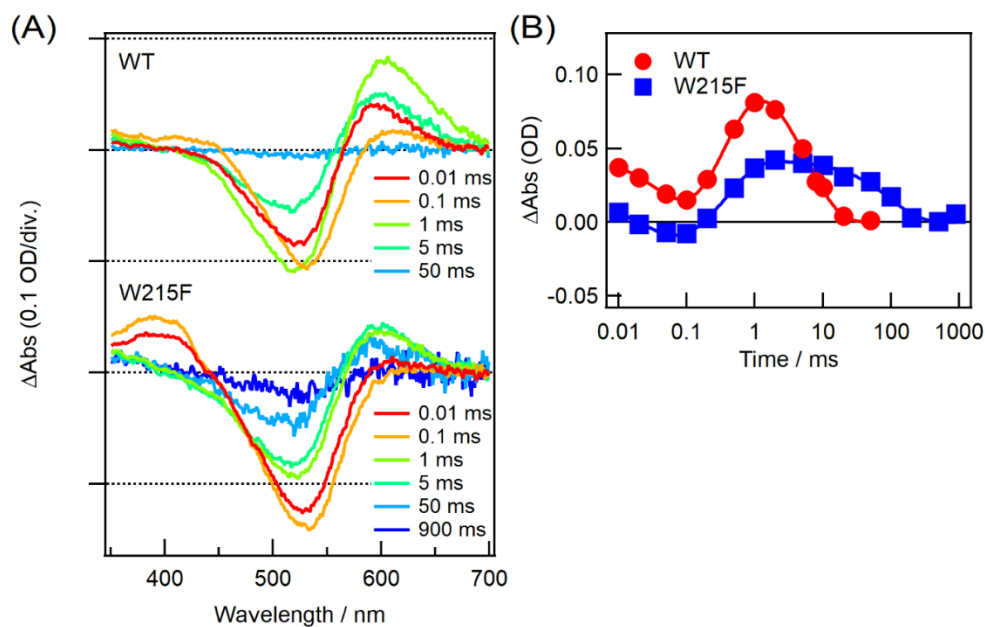
Figure 3 (A) Transient absorption spectra of WT (top) and W215F (bottom). The delay time corresponding to each color trace is noted at the lower right. (B) Time traces of the difference absorbance at 605 nm of WT (red circles) and 600 nm of W215F (blue squares). The solid lines indicate the fitting curves assuming three time constants.
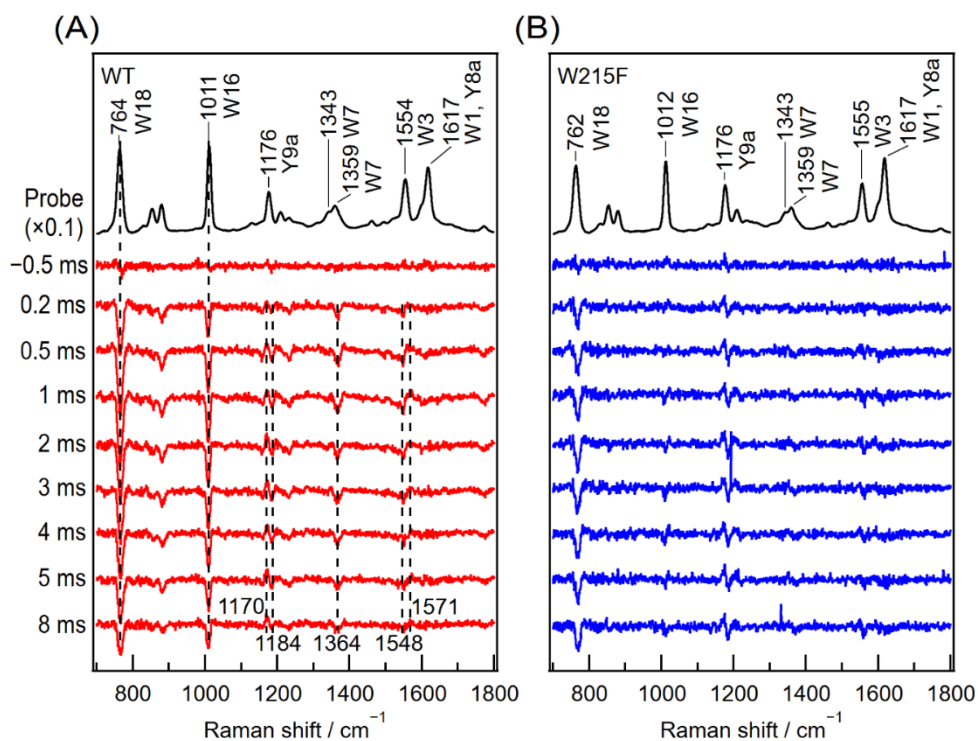

Figure 4 UVRR spectra of WT (A) and W215F (B). The probe and pump lights were 532 and 233 nm, respectively. The spectral contributions of the buffer and quartz cell were subtracted. The top black traces are the unphotolyzed UVRR spectra measured by only probe light multiplied by a factor of 0.1. The red and blue traces are time-resolved difference spectra obtained by subtracting the spectrum of the unphotolyzed state from the pump-probe spectrum at each delay time.
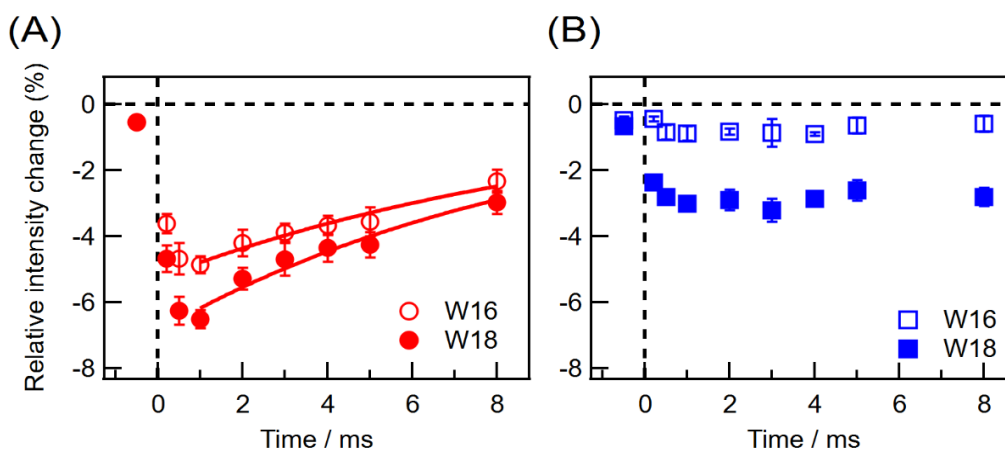
Figure 5 Temporal relative intensity changes of the W16 and W18 bands observed in the UVRR spectra of WT (A) and W215F (B). The solid red lines indicate the fitting curve ranging from 1 to 8 ms, assuming single exponential decay of the O intermediate. The error bars represent standard errors (N=7 and 5 for WT and W215F, respectively).

because their Raman intensity is affected by solvatochromic parameters [28]. Upon 233-nm excitation, increased hydrophobicity around the Trp residues increases the W16 and W18 band intensities [28,37,40]. The transient absorption spectra showed that the O intermediate population becomes maximum at 1 ms and then decays to the unphotolyzed state, with a time constant of 6.3 ms (Figure 3B and Table 1). Thus, the observed intensity changes in the W16 and W18 bands may reflect the formation and decay of the O intermediate, and the environment around either Trp residue is less hydrophobic at 1 ms than at the unphotolyzed state. The doublet W7 band is known to be sensitive to environmental hydrophobicity, which induces an increase in the intensity ratio of I_{1360}/I_{1340} [28,41]. In the difference UVRR spectra, a negative band at 1364 cm^{-1} was observed, indicating decreased hydrophobicity around the Trp residues, in good agreement with the intensity change seen in the W16 and W18 bands. The observed derivative shape in the W3 region (negative and positive peaks at 1548 and 1571 cm^{-1}, respectively) showed a high-frequency shift of the W3 band. Since the frequency of the W3 band reflects the dihedral angle ($\chi^{2,1}$) of Trp residues [42,43], this result indicated that the orientation of the Trp residues changed in the O intermediate. The derivative-shaped feature observed around 1176 cm^{-1} (positive and negative peaks at 1170 and 1184 cm^{-1}, respectively) indicated a low-frequency shift of the Y9a band. The frequency of the Y9a band is used as a marker of the orientation of the phenolic OH group in the Tyr side chain [44]. The observed low-frequency shift of this band implied changes in the orientation of this phenolic OH group in the O intermediate, possibly due to perturbation of the hydrogen bonding network of either Tyr residue. These spectral analyses indicate that structural changes involving a decrease in hydrophobicity around the Trp residues and changes in orientation of the Trp and Tyr side chains occur in the O intermediate. Because KR2 has seven Trp and fifteen Tyr residues [6], these spectral changes are a summation of the spectral contributions of multiple Trp and Tyr residues.

   The UVRR spectra of the W215F mutant are shown in Figure 4B. In the UVRR spectrum of the unphotolyzed state of W215F (Figure 4B, black), the band positions were almost identical to those of WT, except for slight differences in the relative intensities. This result implied that the effects of mutation on the global protein structure of KR2 in the unphotolyzed state are not remarkable, consistent with the absorption and visible RR spectra (Figure 2B and 2C). In contrast, the spectral changes in the pump-induced difference spectra (Figure 4B, blue) were different from those of WT. The most prominent feature of W215F was the magnitude of the intensity changes of the W16 and W18 bands. The intensity change in both bands in W215F was smaller than in WT. In particular, the intensity change of the W16 band was almost negligible in the mutant. The temporal intensity changes of both bands are represented in Figure 5B. Unlike WT, the relative intensity change appeared to be nearly constant from 0.5 to 8 ms. In addition, no intensity change of the W7 band and no frequency shift of the W3 band was observed in W215F. These results strongly suggest that Trp215 contributes primarily to the spectral changes in the W3, W7, W16, and W18 bands in the WT protein, although other Trp residues must have exhibited spectral responses, as W215F still showed changes in the RR bands in the different spectra. By contrast, the derivative-shaped feature observed around the Y9a band was similar to that of WT, indicating that protein conformational changes other than those around Trp215 were not significantly affected by the W215F mutation. Therefore, we concluded that KR2 undergoes a conformational change that decreases hydrophobicity near the Trp215 residue and causes changes in the orientation of the Trp215 side chain in the O intermediate.

Discussion

The W215F mutation had little effect on the structure of KR2 in the unphotolyzed state, as shown by the absorption, visible RR, and UVRR spectra (Figures 2B, C, and 4). On the other hand, the mutation slowed the photocycle by more than one order of magnitude (Figure 3). The slow photocycle of W215F was consistent with its lower activity compared to WT (Figure 2A) and was mainly caused by changes in O intermediate decay (Figure 3 and Table 1). In KR2, the transition from the O intermediate to the unphotolyzed state involves re-isomerization of the retinal chromophore from 13-*cis* to the all-*trans* form [22]. During relaxation, movement of the C20 methyl group of the retinal chromophore is prominent on the cytoplasmic side of the retinal chromophore. Indeed, the temporal structures of KR2 obtained by time-resolved serial crystallography show the largest distance between the C20 methyl group and $N_{\varepsilon 1}$ and C_{α} of Trp215 at 1 ms, and Trp215 shifts toward the cytoplasmic side and away from the retinal Schiff base (Figure 6 and Table 2) [26]. This structural rearrangement should create space for the Na^+ uptake pathway from the cytoplasmic side, as discussed in detail below. In the O intermediate of WT, it is likely that molecular contact between the bulky side chain of Trp215, especially the six-membered ring, and the C20 methyl group facilitates the relaxation of KR2. In contrast, in the W215F mutant, the smaller Phe side chain should eliminate this steric hindrance between the six-membered ring side of Trp215 and the C20 methyl group, thereby extending the lifetime of the O intermediate.

Gloeobacter rhodopsin (GR) acts as an H^+ pump. The atomic contact between the C20 methyl group and Trp222, a residue comparable to Trp215 in KR2, is crucial for mediating transmission of the sequential structural change [30]. The W222F mutant of GR
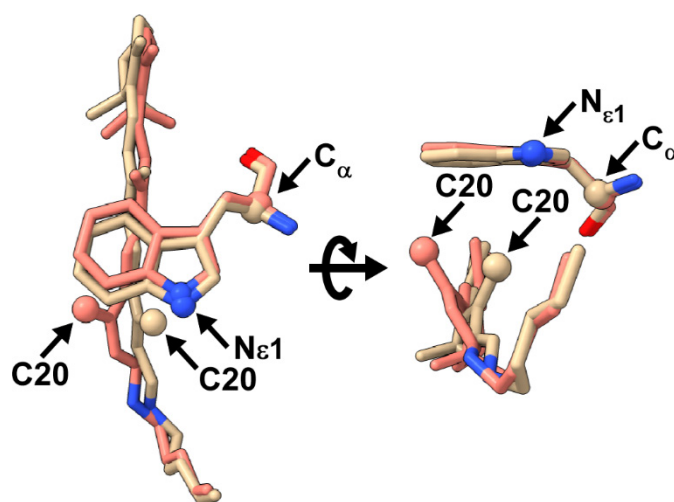

Figure 6 Superposition of structures of the retinal chromophore, including the side chain of Lys255 and Trp215 of KR2 in the unphotolyzed state (gold, PDB ID: 6tk6) and at 1 ms (pink, PDB ID: 6tk2). The C20 methyl group of retinal and $N_{\varepsilon 1}$ and C_{α} of the tryptophan residue are indicated as balls.

Table 2 Distance between the C20 methyl carbon atom of retinal and the atoms of Trp215 determined from the serial crystallographic structures [26]

State (PDB ID)	C20-C_{α}/Å	C20-$N_{\varepsilon 1}$/Å
Unphotolyzed (6tk6)	5.7	4.0
800 fs + 2 ps (6tk5)	6.4	4.0
1 ns + 16 ns (6tk4)	6.8	4.4
30 μs + 150 μs (6tk3)	7.3	4.7
1 ms (6tk2)	7.3	4.8
20 ms (6tk1)	6.9	4.3

shows weak H^+ pumping activity, and its photocycle does not proceed to the M intermediate [30]. In addition, in bacteriorhodopsin from *Halobacterium salinarum* (*Hs*BR), Trp182 is structurally equivalent to Trp215 in KR2 and may be important in the initial conformational changes of the opsin moiety and its involvement in hydrogen bonding with water molecules in various photointermediates [31,38,45]. Therefore, the conserved Trp residue we focused on in this study has important roles in the evolution of conformational changes, acting as a mechanical transducer in microbial rhodopsins even though the mechanism and function vary between species.

Our time-resolved UVRR analysis of WT and W215F revealed that the environment around Trp215 becomes less hydrophobic in the O intermediate than in the unphotolyzed state (Figures 4 and 5). In KR2, the unphotolyzed state is occluded, Na^+ is not bound inside the protein, and Na^+ uptake from the cytoplasmic side occurs during the M-to-O transition [23-26]. The observed decrease in environmental hydrophobicity likely reflects the conformational changes which open a channel connecting the cytoplasmic side to the retinal chromophore. Hence, KR2 forms a transient inward-facing open state during the M-to-O transition. The environment around Trp215 then returns to the original hydrophobic state in the transition from the O intermediate to the unphotolyzed state. The conformational change accompanying hydrophobicity recovery is involved in closing the channel for Na^+ uptake, leading to the next outward-facing-open state. This conformational change is necessary to prevent Na^+ backflow and is consistent with the alternating-access model that is a hallmark of ion pumps [1,46].

Trp215 of KR2 is located on the 6th helix (helix F) [6,13]. In *Hs*BR and sensory rhodopsin II from *Halobacterium salinarum*, the light-induced movements of helix F are likely important to the function of the proteins [47-49]. In particular, an outward tilt of helix F in *Hs*BR is thought to make a transient half-channel for H$^+$ uptake on the cytoplasmic side [47,49,50]. A similar outward tilting motion of helix F in KR2 has been demonstrated by site-directed spin label electronic paramagnetic resonance measurements [51]. These conformational changes in helix F are consistent with our interpretation of transient opening of the channel on the cytoplasmic side around Trp215, and suggest that conformational changes in helix F may be important for the functional expression of microbial rhodopsins in general. However, comparison of the crystal structures of the unphotolyzed state and the O intermediate of KR2 show no noticeable motion of helix F [26]. This discrepancy may be due to the fact that the crystals were prepared from protein in the monomeric state, since KR2 forms a more compact conformation in the monomeric state, especially around the retinal chromophore, than in the pentameric state [16,52]. Also, intermolecular interactions at the oligomeric interface are important to the function and conformation of the protein [21,53,54]. Furthermore, the effect of crystal packing should be also considered as discussed in the serial femtosecond crystallography of *Hs*BR [45]. Future studies of KR2 protein dynamics in the physiological oligomeric state are required to understand the effects of oligomeric state changes in microbial rhodopsins [55,56].

In addition to Trp215, other Trp residues exhibited structural changes in the O intermediate because the W215F mutant showed spectral changes, especially in the W18 band over several milliseconds (Figures 4B and 5B). These changes reflect the less hydrophobic environment in the O intermediate around the Trp residues in general. KR2 has seven Trp residues, of which Trp82, Trp113, and Trp215 are oriented inside the protein. Trp113 is located in the retinal binding pocket of KR2 and on the opposite (extracellular) side of the retinal chromophore to Trp215 [6,13]. Since the side chain of Trp113 forms a transient Na$^+$ binding site in the early O intermediate [26], it is highly likely that this residue largely contributes to the spectral changes observed in the W215F mutant. Trp82 is located on the extracellular side about 20 Å away from the retinal Schiff base [6,13]. Although Trp82 is not directly involved in Na$^+$ transport, its position is in the vicinity of the second transient Na$^+$ binding site on the extracellular side, as revealed by the time-resolved serial crystal structure at 20 ms [26], and near the ion release cavity observed in the freeze-trapped crystal structure of the O intermediate [25]. Therefore, in contrast to Trp215, Trp82 may exhibit conformational changes corresponding to Na$^+$ release. Trp113 and Trp82 may thus contribute to the detected spectral changes in the W215F mutant. The other four Trp residues are located on the surface of KR2 and are unlikely to exhibit conformational changes associated with Na$^+$ transport. However, we cannot completely rule out the possibility that these residues respond during photoactivation due to intermolecular interactions of the oligomeric state of KR2. Our time-resolved UVRR spectra also showed spectral changes derived from Tyr residues (Figure 4), although these changes remain unassigned. Future time-resolved UVRR experiments of KR2 with further Trp and Tyr mutants will probe areas of the protein different from that around Trp215 and provide more insights into the mechanisms enabling unidirectional Na$^+$ transport.

Conclusion

In this study, we presented the conformational changes occurring in KR2 during Na$^+$ transport as probed by time-resolved UVRR spectroscopy. Spectral analysis of WT and the W215F mutant indicated that the bulky side chain of Trp215, which is located in the retinal binding pocket and on the cytoplasmic side relative to the retinal chromophore, is critical for the transmission of sequential structural changes. This Trp residue is conserved among many other microbial rhodopsins, suggesting that it may play an essential role in their various functions, as shown in *Hs*BR and GR. Time-resolved difference spectra showed that the hydrophobicity around Trp215 drastically decreased at 1 ms and then recovered with an about 10 ms time constant, accompanied by O-intermediate decay. This conformational change may reflect opening of a transient channel for Na$^+$ uptake and then closing of the channel to prevent ion backflow, compatible with the alternating-access model. We have demonstrated that time-resolved UVRR spectroscopy is a powerful tool to investigate the protein dynamics of microbial rhodopsins during the photocycle, in combination with structural analyses such as X-ray crystallography and cryo-electron microscopy.

Conflict of Interest

All authors declare that they have no conflicts of interest.

Author Contributions

A.O. and Y.M. designed the research. A.O. and M.M. performed experiments and data analysis. K.I. and H.K. contributed to sample preparation. A.O. and Y.M. wrote the manuscript. All authors discussed and commented on the manuscript.

Data Availability

The evidence data generated and/or analyzed during the current study are available from the corresponding author on reasonable request.

Acknowledgements

References

[1] Drew, D., Boudker, O. Shared molecular mechanisms of membrane transporters. Annu. Rev. Biochem. 85, 543-572 (2016). https://doi.org/10.1146/annurev-biochem-060815-014520

[2] Kandori, H. Ion-pumping microbial rhodopsins. Front. Mol. Biosci. 2 (2015). https://doi.org/10.3389/fmolb.2015.00052

[3] Rozenberg, A., Inoue, K., Kandori, H., Béjà, O. Microbial rhodopsins: The last two decades. Annu. Rev. Microbiol. 75, 427-447 (2021). https://doi.org/10.1146/annurev-micro-031721-020452

[4] Ernst, O. P., Lodowski, D. T., Elstner, M., Hegemann, P., Brown, L. S., Kandori, H. Microbial and animal rhodopsins: Structures, functions, and molecular mechanisms. Chem. Rev. 114, 126-163 (2014). https://doi.org/10.1021/cr4003769

[5] Mizutani, Y. Concerted motions and molecular function: What physical chemistry we can learn from light-driven ion-pumping rhodopsins. J. Phys. Chem. B 125, 11812-11819 (2021). https://doi.org/10.1021/acs.jpcb.1c06698

[6] Inoue, K., Ono, H., Abe-Yoshizumi, R., Yoshizawa, S., Ito, H., Kogure, K., et al. A light-driven sodium ion pump in marine bacteria. Nat. Commun. 4, 1678 (2013). https://doi.org/10.1038/ncomms2689

[7] Inoue, K., Ito, S., Kato, Y., Nomura, Y., Shibata, M., Uchihashi, T., et al. A natural light-driven inward proton pump. Nat. Commun. 7, 13415 (2016). https://doi.org/10.1038/ncomms13415

[8] Bulzu, P.-A., Andrei, A.-Ş., Salcher, M. M., Mehrshad, M., Inoue, K., Kandori, H., et al. Casting light on Asgardarchaeota metabolism in a sunlit microoxic niche. Nat. Microbiol. 4, 1129-1137 (2019). https://doi.org/10.1038/s41564-019-0404-y

[9] Niho, A., Yoshizawa, S., Tsukamoto, T., Kurihara, M., Tahara, S., Nakajima, Y., et al. Demonstration of a light-driven SO_4^{2-} transporter and its spectroscopic characteristics. J. Am. Chem. Soc. 139, 4376-4389 (2017). https://doi.org/10.1021/jacs.6b12139

[10] Oesterhelt, D., Stoeckenius, W. Rhodopsin-like protein from the purple membrane of *Halobacterium halobium*. Nat. New Biol. 233, 149-152 (1971). https://doi.org/10.1038/newbio233149a0

[11] Matsuno-Yagi, A., Mukohata, Y. Two possible roles of bacteriorhodopsin; A comparative study of strains of *Halobacterium halobium* differing in pigmentation. Biochem. Biophys. Res. Commun. 78, 237-243 (1977). https://doi.org/10.1016/0006-291X(77)91245-1

[12] Kandori, H., Inoue, K., Tsunoda, S. P. Light-driven sodium-pumping rhodopsin: A new concept of active transport. Chem. Rev. 118, 10646-10658 (2018). https://doi.org/10.1021/acs.chemrev.7b00548

[13] Kato, H. E., Inoue, K., Abe-Yoshizumi, R., Kato, Y., Ono, H., Konno, M., et al. Structural basis for Na^+ transport mechanism by a light-driven Na^+ pump. Nature 521, 48-53 (2015). https://doi.org/10.1038/nature14322

[14] Konno, M., Kato, Y., Kato, H. E., Inoue, K., Nureki, O., Kandori, H. Mutant of a light-driven sodium ion pump can transport cesium ions. J. Phys. Chem. Lett. 7, 51-55 (2016). https://doi.org/10.1021/acs.jpclett.5b02385

[15] Inoue, K., Nomura, Y., Kandori, H. Asymmetric functional conversion of eubacterial light-driven ion pumps. J. Biol. Chem. 291, 9883-9893 (2016). https://doi.org/10.1074/jbc.M116.716498

[16] Gushchin, I., Shevchenko, V., Polovinkin, V., Kovalev, K., Alekseev, A., Round, E., et al. Crystal structure of a light-driven sodium pump. Nat. Struct. Mol. Biol. 22, 390-395 (2015). https://doi.org/10.1038/nsmb.3002

[17] Nomura, Y., Ito, S., Teranishi, M., Ono, H., Inoue, K., Kandori, H. Low-temperature FTIR spectroscopy provides evidence for protein-bound water molecules in eubacterial light-driven ion pumps. Phys. Chem. Chem. Phys. 20, 3165-3171 (2018). https://doi.org/10.1039/c7cp05674e

[18] Hososhima, S., Kandori, H., Tsunoda, S. P. Ion transport activity and optogenetics capability of light-driven Na^+-pump KR2. PLoS One 16, e0256728 (2021). https://doi.org/10.1371/journal.pone.0256728

[19] Nakajima, Y., Pedraza-González, L., Barneschi, L., Inoue, K., Olivucci, M., Kandori, H. Pro219 is an electrostatic color determinant in the light-driven sodium pump KR2. Commun. Biol. 4, 1185 (2021).

https://doi.org/10.1038/s42003-021-02684-z

[20] Shibata, M., Inoue, K., Ikeda, K., Konno, M., Singh, M., Kataoka, C., et al. Oligomeric states of microbial rhodopsins determined by high-speed atomic force microscopy and circular dichroic spectroscopy. Sci. Rep. 8, 8262 (2018). https://doi.org/10.1038/s41598-018-26606-y

[21] Otomo, A., Mizuno, M., Inoue, K., Kandori, H., Mizutani, Y. Allosteric communication with the retinal chromophore upon ion binding in a light-driven sodium ion-pumping rhodopsin. Biochemistry 59, 520-529 (2020). https://doi.org/10.1021/acs.biochem.9b01062

[22] Nishimura, N., Mizuno, M., Kandori, H., Mizutani, Y. Distortion and a strong hydrogen bond in the retinal chromophore enable sodium-ion transport by the sodium-ion pump KR2. J. Phys. Chem. B 123, 3430-3440 (2019). https://doi.org/10.1021/acs.jpcb.9b00928

[23] Kato, Y., Inoue, K., Kandori, H. Kinetic analysis of H^+-Na^+ selectivity in a light-driven Na^+-pumping rhodopsin. J. Phys. Chem. Lett. 6, 5111-5115 (2015). https://doi.org/10.1021/acs.jpclett.5b02371

[24] Murabe, K., Tsukamoto, T., Aizawa, T., Demura, M., Kikukawa, T. Direct detection of the substrate uptake and release reactions of the light-driven sodium-pump rhodopsin. J. Am. Chem. Soc. 142, 16023-16030 (2020). https://doi.org/10.1021/jacs.0c07264

[25] Kovalev, K., Astashkin, R., Gushchin, I., Orekhov, P., Volkov, D., Zinovev, E., et al. Molecular mechanism of light-driven sodium pumping. Nat. Commun. 11, 2137 (2020). https://doi.org/10.1038/s41467-020-16032-y

[26] Skopintsev, P., Ehrenberg, D., Weinert, T., James, D., Kar, R. K., Johnson, P. J. M., et al. Femtosecond-to-millisecond structural changes in a light-driven sodium pump. Nature 583, 314-318 (2020). https://doi.org/10.1038/s41586-020-2307-8

[27] Harada, I., Takeuchi, H. Raman and ultraviolet resonance Raman spectra of proteins and related compounds. Advances in Infrared and Raman Spectroscopy 13, 113-175 (1986).

[28] Chi, Z., Asher, S. A. UV Raman determination of the environment and solvent exposure of Tyr and Trp residues. J. Phys. Chem. B 102, 9595-9602 (1998). https://doi.org/10.1021/jp9828336

[29] Luecke, H., Schobert, B., Cartailler, J.-P., Richter, H.-T., Rosengarth, A., Needleman, R., et al. Coupling photoisomerization of retinal to directional transport in bacteriorhodopsin. J. Mol. Biol. 300, 1237-1255 (2000). https://doi.org/10.1006/jmbi.2000.3884

[30] Shionoya, T., Mizuno, M., Kandori, H., Mizutani, Y. Contact-mediated retinal–opsin coupling enables proton pumping in *Gloeobacter* rhodopsin. J. Phys. Chem. B 126, 7857-7869 (2022). https://doi.org/10.1021/acs.jpcb.2c04208

[31] Hashimoto, S., Obata, K., Takeuchi, H., Needleman, R., Lanyi, J. K. Ultraviolet resonance Raman spectra of Trp-182 and Trp-189 in bacteriorhodopsin: Novel information on the structure of Trp-182 and its steric interaction with retinal. Biochemistry 36, 11583-11590 (1997). https://doi.org/10.1021/bi971404f

[32] Smith, S. O., Braiman, M. S., Myers, A. B., Pardoen, J. A., Courtin, J. M. L., Winkel, C., et al. Vibrational analysis of the *all-trans*-retinal chromophore in light-adapted bacteriorhodopsin. J. Am. Chem. Soc. 109, 3108-3125 (1987). https://doi.org/10.1021/ja00244a038

[33] Smith, S. O., Pardoen, J. A., Lugtenburg, J., Mathies, R. A. Vibrational analysis of the 13-*cis*-retinal chromophore in dark-adapted bacteriorhodopsin. J. Phys. Chem. 91, 804-819 (1987). https://doi.org/10.1021/j100288a011

[34] Smith, S. O., Lugtenburg, J., Mathies, R. A. Determination of retinal chromophore structure in bacteriorhodopsin with resonance Raman spectroscopy. J. Membr. Biol. 85, 95-109 (1985). https://doi.org/10.1007/BF01871263

[35] Smith, S. O., Myers, A. B., Pardoen, J. A., Winkel, C., Mulder, P. P., Lugtenburg, J., et al. Determination of retinal Schiff base configuration in bacteriorhodopsin. Proc. Natl. Acad. Sci. U.S.A. 81, 2055-2059 (1984). https://doi.org/10.1073/pnas.81.7.2055

[36] Oladepo, S. A., Xiong, K., Hong, Z., Asher, S. A., Handen, J., Lednev, I. K. UV resonance Raman investigations of peptide and protein structure and dynamics. Chem. Rev. 112, 2604-2628 (2012). https://doi.org/10.1021/cr200198a

[37] Takeuchi, H. UV Raman markers for structural analysis of aromatic side chains in proteins. Anal. Sci. 27, 1077-1086 (2011). https://doi.org/10.2116/analsci.27.1077

[38] Hashimoto, S., Sasaki, M., Takeuchi, H., Needleman, R., Lanyi, J. K. Changes in hydrogen bonding and environment of tryptophan residues on helix F of bacteriorhodopsin during the photocycle: A time-resolved ultraviolet resonance Raman study. Biochemistry 41, 6495-6503 (2002). https://doi.org/10.1021/bi012190b

[39] Mizuno, M., Shimoo, Y., Kandori, H., Mizutani, Y. Effect of a bound anion on the structure and dynamics of halorhodopsin from *Natronomonas pharaonis*. Struct. Dyn. 6, 054703 (2019). https://doi.org/10.1063/1.5125621

[40] Matsuno, M., Takeuchi, H. Effects of hydrogen bonding and hydrophobic interactions on the ultraviolet resonance Raman intensities of indole ring vibrations. Bull. Chem. Soc. Jpn. 71, 851-857 (1998). https://doi.org/10.1246/bcsj.71.851

[41] Harada, I., Yamagishi, T., Uchida, K., Takeuchi, H. Ultraviolet resonance Raman spectra of bacteriorhodopsin in

the light-adapted and dark-adapted states. J. Am. Chem. Soc. 112, 2443-2445 (1990). https://doi.org/10.1021/ja00162a068

[42] Juszczak, L. J., Desamero, R. Z. B. Extension of the tryptophan $\chi^{2,1}$ dihedral angle−W3 band frequency relationship to a full rotation: Correlations and caveats. Biochemistry 48, 2777-2787 (2009). https://doi.org/10.1021/bi801293v

[43] Miura, T., Takeuchi, H., Harada, I. Tryptophan Raman bands sensitive to hydrogen bonding and side-chain conformation. J. Raman Spectrosc. 20, 667-671 (1989). https://doi.org/10.1002/jrs.1250201007

[44] Takeuchi, H., Watanabe, N., Satoh, Y., Harada, I. Effects of hydrogen bonding on the tyrosine Raman bands in the 1300–1150 cm^{-1} region. J. Raman Spectrosc. 20, 233-237 (1989). https://doi.org/10.1002/jrs.1250200407

[45] Nango, E., Royant, A., Kubo, M., Nakane, T., Wickstrand, C., Kimura, T., et al. A three-dimensional movie of structural changes in bacteriorhodopsin. Science 354, 1552-1557 (2016). https://doi.org/10.1126/science.aah3497

[46] Tanford, C. Mechanism of free energy coupling in active transport. Annu. Rev. Biochem. 52, 379-409 (1983). https://doi.org/10.1146/annurev.bi.52.070183.002115

[47] Weinert, T., Skopintsev, P., James, D., Dworkowski, F., Panepucci, E., Kekilli, D., et al. Proton uptake mechanism in bacteriorhodopsin captured by serial synchrotron crystallography. Science 365, 61-65 (2019). https://doi.org/10.1126/science.aaw8634

[48] Sasaki, J., Tsai, A.-l., Spudich, J. L. Opposite displacement of helix F in attractant and repellent signaling by sensory rhodopsin-Htr complexes. J. Biol. Chem. 286, 18868-18877 (2011). https://doi.org/10.1074/jbc.M110.200345

[49] Sass, H. J., Büldt, G., Gessenich, R., Hehn, D., Neff, D., Schlesinger, R., et al. Structural alterations for proton translocation in the M state of wild-type bacteriorhodopsin. Nature 406, 649-653 (2000). https://doi.org/10.1038/35020607

[50] Radzwill, N., Gerwert, K., Steinhoff, H.-J. Time-resolved detection of transient movement of helices F and G in doubly spin-labeled bacteriorhodopsin. Biophys. J. 80, 2856-2866 (2001). https://doi.org/10.1016/S0006-3495(01)76252-2

[51] da Silva, G. F., Goblirsch, B. R., Tsai, A. L., Spudich, J. L. Cation-specific conformations in a dual-function ion-pumping microbial rhodopsin. Biochemistry 54, 3950-3959 (2015). https://doi.org/10.1021/bi501386d

[52] Kovalev, K., Polovinkin, V., Gushchin, I., Alekseev, A., Shevchenko, V., Borshchevskiy, V., et al. Structure and mechanisms of sodium-pumping KR2 rhodopsin. Sci. Adv. 5, eaav2671 (2019). https://doi.org/10.1126/sciadv.aav2671

[53] Shigeta, A., Ito, S., Kaneko, R., Tomida, S., Inoue, K., Kandori, H., et al. Long-distance perturbation on Schiff base-counterion interactions by His30 and the extracellular Na^+-binding site in *Krokinobacter* rhodopsin 2. Phys. Chem. Chem. Phys. 20, 8450-8455 (2018). https://doi.org/10.1039/c8cp00626a

[54] Kaur, J., Kriebel, C. N., Eberhardt, P., Jakdetchai, O., Leeder, A. J., Weber, I., et al. Solid-state NMR analysis of the sodium pump *Krokinobacter* rhodopsin 2 and its H30A mutant. J. Struct. Biol. 206, 55-65 (2018). https://doi.org/10.1016/j.jsb.2018.06.001

[55] Hussain, S., Kinnebrew, M., Schonenbach, N. S., Aye, E., Han, S. Functional consequences of the oligomeric assembly of proteorhodopsin. J. Mol. Biol. 427, 1278-1290 (2015). https://doi.org/10.1016/j.jmb.2015.01.004

[56] Iizuka, A., Kajimoto, K., Fujisawa, T., Tsukamoto, T., Aizawa, T., Kamo, N., et al. Functional importance of the oligomer formation of the cyanobacterial H^+ pump *Gloeobacter* rhodopsin. Sci. Rep. 9, 10711 (2019). https://doi.org/10.1038/s41598-019-47178-5